energies

MDPI

Article

Experimental Hardware-in-the-Loop Assessment of Automatic Voltage Regulator Mismatch Effects in Parallel-Operating Shipboard Generators

Tymoteusz Zaleski [1], Dariusz Tarnapowicz [1,*], Zbigniew Matuszak [2], Marek Jaśkiewicz [3] and Radoslaw Ptak [1]

[1] Faculty of Mechatronics and Electrical Engineering, Maritime University of Szczecin, 71-650 Szczecin, Poland; t.zaleski@pm.szczecin.pl (T.Z.); 31129@s.pm.szczecin.pl (R.P.)
[2] Faculty of Marine Engineering, Maritime University of Szczecin, 71-650 Szczecin, Poland; z.matuszak@pm.szczecin.pl
[3] Faculty of Mechatronics and Mechanical Engineering, Kielce University of Technology, 25-314 Kielce, Poland; m.jaskiewicz@tu.kielce.pl
* Correspondence: d.tarnapowicz@pm.szczecin.pl; Tel.: +48-9148-09-955

Abstract

Parallel operation of synchronous generators in a shipboard power system requires properly coordinated Automatic Voltage Regulators (AVRs). AVR mismatch can cause unequal reactive power sharing and increased generator currents. In operational and service practice, the possibilities for safe and repeatable diagnosis of AVR settings under parallel-operation conditions are limited. Conventional workshop tests do not reproduce the complete coupling between the regulators, common-bus voltage, stator currents, and reactive power flow. This paper presents the development and experimental assessment of a Hardware-in-the-Loop platform for testing two physical digital AVRs coupled to real-time models of two synchronous generators, prime movers, a common main switchboard (MSB), and a load. The platform uses a common voltage interface and inverter-based stator-current reproduction interfaces. The current-reproduction interface was functionally validated. A reference operating test and tests of the effects of differences in proportional gain, integral time, voltage reference, and voltage droop settings were performed. Matched AVR settings provided stable operation following load changes. Mismatched voltage references and voltage droop settings caused persistent unequal reactive power sharing. Zero voltage droop caused oscillatory reactive power exchange and increased generator currents. The platform enables safe and repeatable assessment of physical AVRs during parallel generator operation without the use of high-power synchronous generators.

Keywords: automatic voltage regulator; hardware-in-the-loop; shipboard power system; parallel synchronous generators; reactive power sharing; voltage droop; excitation control; generator diagnostics

Check for updates

Academic Editor: Branislav Hredzak

Received: 1 October 2026
Revised: 9 November 2026
Accepted: 18 November 2026
Published: 20 November 2026

Copyright: © 2026 by the authors. Licensee MDPI, Basel, Switzerland. This article is an open access article distributed under the terms and conditions of the Creative Commons Attribution (CC BY) license.

1. Introduction

The shipboard electrical power system is one of the principal technical systems determining the safety and continuity of vessel operation. It supplies auxiliary propulsion loads, steering equipment, pumps, navigation and communication systems, cargo-handling equipment, and other loads required for safe navigation. Unlike extensive land-based power systems, a shipboard network usually operates as an autonomous or islanded system. It includes a limited number of generating sets connected to a common main switchboard (MSB). The ratings of large loads can be comparable to the rating of a single generating

set. Consequently, shipboard systems are often described as soft or weak networks. They are susceptible to voltage and frequency deviations caused by load changes or changes in source operating conditions [1–6]. Operating conditions are particularly variable during vessel manoeuvring. Switching loads on and off and changes in generating-set loading affect the instantaneous power balance and operating conditions of the shipboard power plant [7]. On many vessels, the main power sources are diesel-engine-driven synchronous generators with electromagnetic excitation systems. Two or more generating sets often operate in parallel on a common MSB [1,2,5,8]. This configuration accommodates varying power demand, provides reserve capacity, and maintains continuity of supply after the failure or disconnection of one source. Depending on the operating mode, a vessel can also use shore power while berthed. Transfer between autonomous shipboard power-plant operation and supply from the national grid requires suitable synchronisation, coordinated switching, and uninterrupted supply to shipboard loads [9]. Parallel operation of voltage sources is substantially more complex than operation of an individual generator. Generators connected to a common bus are electrically coupled. A change in the excitation of one generator affects reactive power flow, armature currents, and the operating conditions of the remaining units [10–13].

Active power sharing and reactive power sharing among parallel generators are governed by different control loops. Active power sharing depends primarily on the mechanical power of the prime movers and on the speed droop characteristics of their governors. Reactive power sharing depends directly on the excitation systems and Automatic Voltage Regulators (AVRs). In practical operation, the relationship among active power, reactive power, and generator current is also described by the power factor. Its value varies with the type of loads and the operating state of the shipboard network. Correct power-factor identification is important for assessing generating-set loading, efficiency, and available current margin [14]. AVRs use voltage and current signals and, depending on their design, may also use frequency, reactive power, and power-factor signals. These inputs control the excitation current and maintain the required voltage at the generator terminals or at the common bus [15–18]. During parallel operation, AVRs are not independent because they act on the common MSB voltage node. Differences in voltage-reference settings, proportional gain, integral time, measurement signals, and voltage droop characteristics can cause unequal reactive power sharing, circulating currents, and degraded operating stability [10–13,19–23].

The consequences of inadequate AVR coordination are particularly significant in isolated shipboard power systems. A generator with a higher effective voltage reference or a stiffer voltage droop characteristic can assume a disproportionately large share of reactive power, while the other generator may enter underexcited operation. The MSB voltage may remain close to its rated value, while internal reactive power exchange and generator current loading increase. In severely mismatched systems, poorly damped reactive power oscillations, referred to as reactive power hunting, may occur. Excitation limits may be reached, protection devices may operate, available power reserve may be reduced, and the risk of blackout may increase [10–13,19–25].

The significance of interactions between parallel generators was demonstrated in the authors' earlier study on loss of excitation in an autonomous shipboard power plant [24]. That study showed that a change in the excitation of one generator affects the operating points of both machines, reactive power flow, and armature currents. Partial or complete loss of excitation can cause a hazardous current increase in both generating sets. Although loss of excitation is a fault condition, a similar interaction mechanism occurs when both generators and their AVRs are operational but their settings are not properly coordinated. Therefore, AVR mismatch should be regarded not only as a commissioning-quality issue but also as an operating condition with potential safety implications.

Modern digital AVRs provide greater flexibility than conventional analogue regulators. They can perform voltage control, reactive power or power-factor control, voltage droop functions, excitation limiting, frequency-dependent functions, protection functions, and diagnostics [15–18,25]. However, the large number of parameters increases the need for correct setting and verification after repair, replacement, or commissioning. Full-scale testing of AVRs on an operating vessel is usually impractical or unjustified. Intentional changes in droop settings, voltage references, reactive power sharing, or large load steps can disturb continuity of supply and create risks for safety-critical loads. Conventional workshop tests using a three-phase autotransformer also do not provide a complete assessment of a digital AVR. They do not reproduce the closed-loop relationship among excitation, the generator, stator currents, reactive power, and the common bus. In the authors' preliminary tests, reducing the autotransformer voltage below the reference value did not produce the expected increase in the excitation current of the tested digital AVR.

Hardware-in-the-Loop (HIL) technology retains the AVR under test as physical hardware while generators, prime movers, loads, and the electrical network are represented by a real-time model. The regulator therefore receives physical voltage and current signals corresponding to the instantaneous state of the modelled system. Its excitation output is fed back into the model. HIL, real-time HIL, and power HIL methods have been used to investigate AVRs, excitation systems, limiters, protection functions of synchronous generators, and control systems in microgrids [26–38]. These methods support repeatable and safe testing of dynamic conditions without using a high-power physical generator or interfering with an operating shipboard installation.

In more recent studies, HIL technology has been used to diagnose physical static excitation systems of synchronous generators under both normal operating and fault conditions [39]. Power hardware-in-the-loop (PHIL) platforms are also being developed to emulate synchronous generators in autonomous power generation systems and reproduce their responses to changes in active and reactive loads while accounting for magnetic nonlinearities [40,41]. These studies are complemented by recent reviews of HIL/PHIL platform architectures, hardware interfaces, and limitations related to stability and reproduction accuracy [42,43].

Unlike the studies discussed above, which focus on generator emulation or the diagnosis of a single excitation system, the present work focuses on experimentally assessing the effects of setting mismatches between two physical AVRs coupled to models of shipboard generators operating in parallel.

The authors previously developed an HIL platform for testing a physical AVR coupled to a model of a standalone shipboard synchronous generator [26]. The study confirmed that voltage control could be assessed under steady-state conditions and dynamic load changes without using an actual generator. However, it did not reproduce the principal issue of a multi-source shipboard power system: coupling of the voltage-control loops of two AVRs through a common MSB. The literature reports reactive power-sharing methods for shipboard microgrids based on droop control, hierarchical control, virtual-impedance control, and advanced control algorithms [19–23,44–46]. These studies primarily address power-electronic sources and microgrid-control algorithms. They do not experimentally assess two physical commercial digital AVRs coupled to synchronous generators in a closed-loop HIL system.

Based on the literature review, no experimental HIL studies were identified that systematically assessed the effect of parameter mismatch between two physical digital AVRs on the parallel operation of synchronous generators in an isolated shipboard power system. This applies in particular to the effects of differences in proportional gain, integral time, voltage-reference setting, and voltage droop characteristic on transient and steady-state

reactive power sharing. Therefore, this study develops and experimentally evaluates a real-time HIL platform for investigating the effect of AVR mismatch on two parallel-operating shipboard synchronous generators. Both digital AVRs are retained as physical hardware. The generators, prime movers, load, and MSB are represented by a real-time model.

The main contributions of this work are as follows:

Development of a real-time HIL platform for testing two physical digital AVRs coupled to a model of parallel-operating shipboard synchronous generators, a common MSB, and a load.

Development and functional validation of an HIL hardware interface for physical reproduction of stator currents generated by the real-time model. The interface provides the physical AVRs with representative current signals required for voltage droop operation and reactive power sharing.

Experimental assessment of the effects of differences in proportional gain K_p, integral time, voltage-reference setting, and voltage droop setting on MSB voltage, active power, reactive power, excitation currents, and generator currents.

Demonstration that AVR-setting mismatch can cause unequal reactive power sharing, circulating currents, and poorly damped reactive power oscillations, even when the generators are correctly synchronised and the MSB voltage appears normal.

Presentation of a practical method for diagnostic testing, post-repair verification, commissioning, and safe functional testing of digital AVRs intended for parallel operation with megawatt-class shipboard generators.

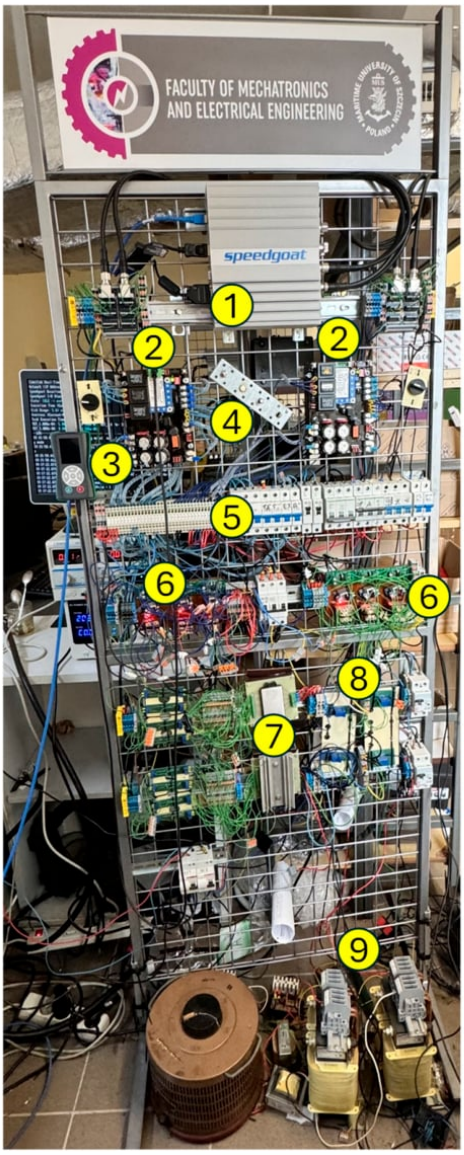
The remainder of this paper is organised as follows. Section 2 describes the HIL platform architecture, real-time model, AVRs, hardware interfaces, and test scenarios. Section 3 presents the results for the reference operating condition and for cases with mismatched AVR settings. Section 4 discusses the interaction mechanisms between the regulators and the relevance of the proposed method to testing, commissioning, and servicing shipboard automation systems. Section 5 presents the main conclusions.

2. Materials and Methods

This study uses HIL technology to investigate two physical digital AVRs coupled to a model of two parallel-operating shipboard synchronous generators. The real-time model represents the generators, prime movers, MSB, and dynamic load. The AVRs, voltage and current interfaces, and measurement circuits are physical components of the test platform.

Figure 1 shows the laboratory implementation of the test platform. It includes a Speedgoat platform (Speedgoat, Liebefeld, Switzerland), two LXCOS digital AVRs (EMRI Services, Ede, The Netherlands), signal-amplification and conditioning circuits, current-controlled inverters, excitation-current measurement circuits, switching equipment, protective devices, and auxiliary power supplies. The platform enables repeatable tests without the use of physical megawatt-class generators.

Figure 2 presents the functional architecture of the platform. The upper part of the diagram shows the real-time simulation environment based on MATLAB/Simulink R2024b (MathWorks, Natick, MA, USA) with Simulink Real-Time and the Speedgoat I/O Blockset) and Speedgoat. It includes two prime-mover models with speed governors and speed droop functions, two synchronous-generator models, a common MSB, and active and reactive-load models. The lower part shows the physical HIL. It includes two hysteresis-controlled inverters, a common MSB voltage-feedback interface, and two physical AVRs.



1 – Real-time simulator (Speedgoat)

2 –Physical digital AVRs units

3 - LCD display panel

4 – Voltage Setpoints

5 – terminal block and switches

6 – Voltage signal-conditioning interface

7 - Intelligent Power Modules (IPMs)

8 - Current transducers for inverter control and excitation-current feedback

9 - Inverter output inductors

Figure 1. Experimental laboratory platform for HIL testing of two physical digital AVRs in a parallel shipboard generator system.

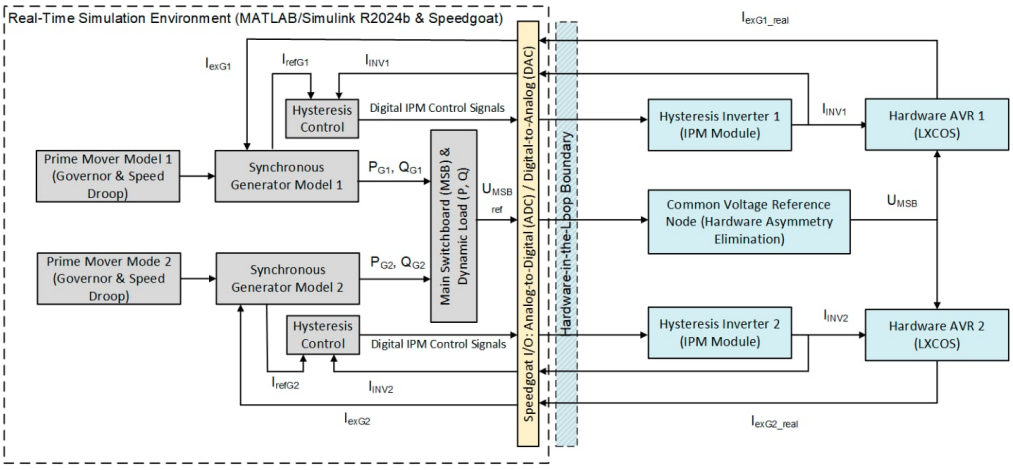


Figure 2. Functional architecture of the real-time HIL platform for testing two physical digital AVRs in parallel-operating shipboard synchronous generators.

2.1. Parallel Generator Model

The real-time model represents an autonomous shipboard power system with two synchronous generators connected in parallel to a common MSB. Each generating set comprises a prime-mover model, a speed governor, a synchronous-generator model, and a physical AVR connected through the HIL interface. The speed governors, through their droop characteristics, determine active power sharing, whereas the physical AVRs regulate excitation and affect reactive power sharing. The generator models calculate phase voltages, stator currents, active power, reactive power, rotational speed, and excitation-related variables. The active and reactive load can be varied in real time. This enables the reproduction of load steps and severe inductive conditions associated with the operation of large shipboard loads. PI speed controllers with 5% speed droop were included in the prime-mover models to maintain stable active-power sharing between the generators. The droop term reduced the speed reference in proportion to active-power loading, with a reduction of 5% of the rated speed at the rated active power P_n. The proportional and integral settings entered in the controller blocks were $P = 10^7$ and $I = 10^7$, respectively. These settings were selected experimentally to obtain stable operation of the investigated HIL configuration. The design and optimisation of the speed controllers were outside the scope of this study.

The load was represented by multiple standard Three-Phase Parallel RLC Load blocks, configured as grounded-wye loads with a nominal line-to-line voltage of 400 V and a nominal frequency of 50 Hz. Step changes in active and reactive loading were implemented by connecting additional load branches in parallel with the base load through circuit breakers, according to the test scenarios described in Section 2.5.

The predefined "11:50 Hz 400 V 1320 kVA 1500 RPM" parameter set of the Synchronous Machine SI Fundamental block was used without modification. The objective was to demonstrate the applicability of the developed HIL platform to assessing the interaction of physical AVRs, rather than to reproduce a specific physical generator. The parameters of the adopted model are listed in Table 1. When applying the platform to AVRs intended for a particular generating set, the model should be parameterized using data representative of that generating set.

Table 1. Parameters of the synchronous generator model.

Parameter	Symbol	Value
Rated apparent power	S_n	1320 kVA
Rated line-to-line voltage	U_n	400 V (RMS)
Rated line current	I_n	1905 A (RMS)
Rated frequency	f_n	50 Hz
Rated rotational speed	n_n	1500 rpm
Rotor type	-	Salient-pole
Number of pole pairs	p	2
Rotor inertia	J	33.01 kg·m^2
Stator resistance	R_s	1.600×10^{-3} Ω
Stator leakage inductance	L_l	1.543×10^{-5} H
d- and q-axis magnetising inductances	L_{md}; L_{mq}	1.057×10^{-3} H; 7.755×10^{-4} H
Field winding resistance and leakage inductance	R_f'; L_{lfd}'	3.828×10^{-4} Ω; 1.815×10^{-4} H
d-axis damper resistance and leakage inductance	R_{kd}'; L_{lkd}'	2.489×10^{-2} Ω; 8.695×10^{-4} H
q-axis damper resistance and leakage inductance	R_{kq1}'; L_{lkq1}'	2.893×10^{-3} Ω; 7.165×10^{-5} H
Viscous friction coefficient	F	0.63 N·m·s

The generator model was parameterized using winding resistances and inductances, as reported in Table 1, rather than by directly specifying transient time constants. In Table 1, primed rotor quantities are referred to the stator, and values grouped within a single row

follow the order of the corresponding symbols. At the rated frequency, the synchronous reactances calculated from the model inductances are $X_d = 0.336914\,\Omega$ and $X_q = 0.248478\,\Omega$, while the stator leakage reactance is $X_l = 0.00484748\,\Omega$.

2.2. Physical AVRs and HIL Interfaces

Two physical LXCOS digital AVRs were used in the study. Each regulator receives a three-phase voltage signal representing the common MSB voltage and a current signal representing the current of its assigned generator. The AVRs implement voltage droop by quadrature droop compensation, in which the voltage correction depends on the reactive component of the generator current. The AVR excitation-current output is measured and fed back to the real-time model as the excitation input of the corresponding generator. The voltage interface reproduces the three-phase voltage required by the AVR measurement circuits. Analogue signals from the Speedgoat module are amplified by a factor of two [26] and adjusted to the required voltage level. A single common voltage-reproduction interface supplies both AVRs with three-phase voltage signals representing the modelled MSB voltage. This arrangement was adopted instead of two separate voltage-reproduction channels to avoid differences between the voltage signals supplied to the two regulators.

2.3. Voltage Interface and Excitation Current Coupling

The hardware implementation of the voltage reproduction path and the excitation current feedback measurement path was described in the authors' previous study on HIL testing of a single AVR [26]. These solutions were retained in the present test platform, which was extended to include a second physical AVR and a corresponding excitation current measurement channel. Both AVRs receive voltage signals representing the voltage of the common MSB.

The voltage interface physically reproduces the three-phase voltage signals required by the AVR measurement circuits. Phase voltages calculated by the real-time model are transmitted through the analogue outputs of the Speedgoat system to signal-conditioning and amplification circuits. These circuits adapt the signal levels to the measurement-input ranges of the AVRs while preserving the amplitude, frequency, phase sequence, and timing relationships defined by the model.

Both AVRs are connected to a common voltage-feedback interface representing the MSB voltage. This arrangement ensures that both regulators respond to the voltage at the same common electrical node of the modelled parallel system. It also reduces unintended differences between the voltage paths supplied to the two AVRs. Such differences could otherwise be interpreted as a voltage-reference mismatch or as an effect of regulator mismatch.

The excitation current supplied by each physical AVR is measured using a current transducer. The transducer output is connected to an analogue input of the Speedgoat system, scaled, and used as an input to the generator model. The scaling was selected so that the nominal excitation current corresponds to the rated terminal voltage of 400 V under nominal conditions. A voltage change in the model changes the voltage signal supplied to the AVR input. The AVR then changes the physical excitation current. The measured excitation current modifies the electromagnetic state of the corresponding generator in the real-time model. This establishes closed-loop HIL operation.

2.4. Current-Reproduction Interface

This section describes the stator current reproduction interfaces that provide the physical current signals required by the AVRs during tests of parallel generator operation.

In the HIL model, generator stator currents are computed numerically, so they do not naturally exist as physical currents in the AVR input circuits. In a real parallel-operated

system, the generator current signal, typically obtained from a current transformer or an equivalent measurement circuit, can be used by the AVR to implement voltage droop and reactive power sharing. To reproduce this coupling, two independent hysteresis-controlled current-source inverter interfaces were developed. Figure 3 shows the functional block diagram of one stator current reproduction channel. The second channel, serving the second AVR, has the same structure.

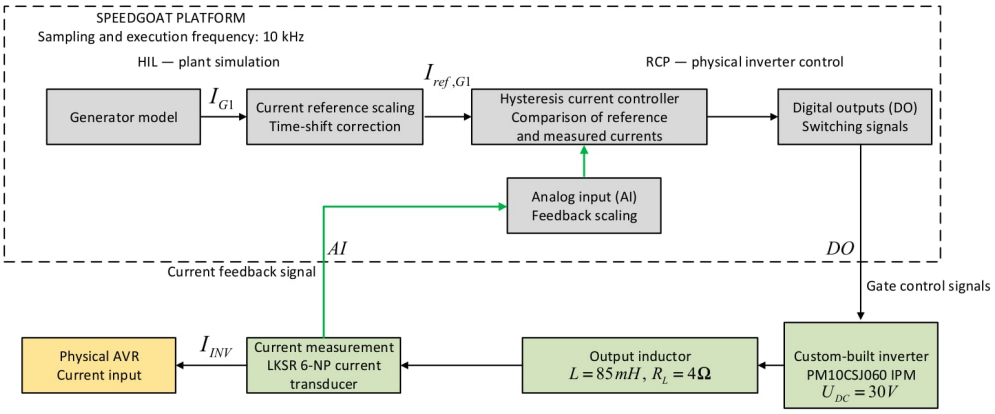


Figure 3. Functional block diagram of the stator-current reproduction interface with hysteresis current control implemented on the Speedgoat platform.

The generator model calculates the stator current, which, after scaling and time-shift correction, serves as the reference current for the hysteresis controller. Scaling adapts the current calculated by the model to the range physically reproduced at the AVR current input.

The scaling factor was selected so that the rated generator current of 1905 A (RMS) corresponded to an inverter output current of $I_{INV} = 0.5$ A RMS. This factor is given by:

$$k_I = \frac{I_{INV,N}}{I_N} = \frac{0.5}{1905} = \frac{1}{3810}, \tag{1}$$

The instantaneous currents of both generators are scaled according to the following equation:

$$i^{(0)}_{ref,Gj}[k] = k_I i_{Gj}[k] = \frac{i_{Gj}}{3810},\ j \in \{1,2\}, \tag{2}$$

where $i_{Gj}[k]$ denotes the instantaneous stator current of generator G_j calculated by the real-time model, and k is the sample index. The symbol $i^0_{\mathrm{ref},Gj}[k]$ denotes the scaled reference current before time-shift correction. After this correction, the signal $i_{\mathrm{ref},Gj}[k]$ is supplied to the hysteresis controller of the corresponding inverter.

The physical output current of each inverter is measured using an LKSR 6-NP current transducer. Instantaneous input currents from −6 A to +6 A correspond to output voltages from 1.875 V to 3.125 V, with 2.5 V corresponding to zero current. The voltage signal is supplied to an analogue input (AI) of the Speedgoat platform.

In the real-time model, the zero-current offset voltage U_0 is subtracted from the measured transducer voltage, and the resulting difference is multiplied by a conversion factor. The measured inverter current is calculated using the following equation:

$$i_{INV,j}[k] = K_{LEM}(u_{LEM,j}[k] - U_0),\ j \in \{1,2\}, \tag{3}$$

where

$$U_0 = 2.5\ \mathrm{V},\ K_{LEM} = 9.6\ \mathrm{A/V}, \tag{4}$$

The symbol $u_{\mathrm{LEM},j}[k]$ denotes the transducer output voltage read through an analogue input of the Speedgoat platform, U_0 is the voltage corresponding to zero current, and K_{LEM}

is the conversion factor used in the model. The resulting signal $i_{\mathrm{INV},j}[k]$ represents the measured inverter current in amperes and is compared with the reference current $i_{\mathrm{ref},Gj}[k]$ in the hysteresis controller. Based on this comparison, switching signals are generated and transmitted to the inverter through the digital outputs (DO) of the Speedgoat platform.

The inverter, built using a PM10CSJ060 intelligent power module (IPM), is supplied with a DC voltage of 30 V. Its output circuit includes an inductor with an inductance of 85 mH and a winding resistance of 4 Ω. The inverter produces the physical current supplied to the AVR current input. The real-time model, hysteresis controller, and Speedgoat input/output modules operate at 10 kHz, corresponding to a time step of 100 µs. The controller uses symmetrical switching thresholds corresponding to current deviations of ±10 mA from the reference, giving a total hysteresis band width of 20 mA.

For each current reproduction channel, the control error is defined as the difference between the reference current and the measured inverter current:

$$e_j[k] = i_{ref,Gj}[k] - i_{INV,j}[k],\ j \in \{1,2\}, \tag{5}$$

where k is the sample index, and j identifies the channel corresponding to generator G_1 or G_2. Both current signals are expressed in amperes after applying the scaling described above.

The operation of the hysteresis controller is described by the following equation:

$$q_I[k] = \begin{cases} +1, & e_j[k] \geq h, \\ -1, & -1e_j[k] \geq h, \\ q_j[k-1], & -h < e_j[k] < h, \end{cases} \tag{6}$$

where $h = 10$ mA is half of the hysteresis band width. The state $q_j = +1$ selects the inverter switching configuration that increases the current, whereas $q_j = -1$ selects the configuration that decreases it. Within the hysteresis band, the previous switching state is retained.

A correct phase relationship between the current signal and the voltage supplied to the AVR measurement inputs is critical. The voltage and current reproduction paths include conditioning, amplification, transformation, and control stages that introduce different time delays. Without compensation, the AVR may interpret the power factor differently from the real-time model, because the physical current I_{INV} is phase-shifted relative to the physically reproduced voltage U_{MSB}. Such a phase mismatch can lead to incorrect interpretation of the reactive current component by the AVR and, consequently, degrade reactive power sharing. To compensate for the phase shift introduced by the voltage and current reproduction paths, a time delay was applied to the current-reference signal. A delay of 5.7 ms was selected experimentally by comparing the power factor calculated in the real-time model with the value indicated on the LCD panel of the physical AVR. Agreement between these values is therefore important for the operation of the voltage droop function.

For each generator, the stator current calculated in the real-time model is scaled and corrected for the time shift to form the reference signal for the corresponding hysteresis controller. The controller compares this signal with the measured inverter output current and generates switching signals for the inverter, which are transmitted through the digital outputs of the Speedgoat platform. The physical output current of each inverter is supplied through a series output inductor to the current input of the corresponding AVR. No external current transformer is used between the inverter and the AVR. Galvanically isolated power-electronic stages with current limiting and protection were used to ensure safe operation under the tested conditions.

In the presented architecture, the Speedgoat platform simultaneously runs the generator model in HIL mode and controls the physical inverter in Rapid Control Prototyping (RCP) mode.

The operation of the current reproduction interface was assessed by comparing the current calculated in the generator model with the physically reproduced inverter current,

accounting for the scaling factor. In addition, the current and power factor values calculated in the model were checked against the readings on the LCD panel of the physical AVR. The validation results are presented in Section 3.1.

2.5. Test Scenarios

The tests were carried out after synchronising the generators, connecting them to the common MSB, and reaching an initial steady state. In the reference case, both AVRs operated with identical, previously tuned settings for proportional gain, integral time, voltage reference, and voltage droop. This case served as the baseline for assessing changes in MSB voltage, active- and reactive power sharing, excitation currents, and generator currents during subsequent tests.

In the reference case, both AVRs operated with identical settings: Vsetpoint = 400 V, Kp = 24%, Ki = 75%, and Voltage droop = 90%. The voltage droop setting of 90% corresponded to a static characteristic slope of 4.5%. The percentage values of Kp, Ki, and the Voltage droop parameter are reported as displayed in the AVR configuration interface, without conversion into controller model coefficients. In the test descriptions, "minimum" and "maximum" denote parameter settings of 0% and 100%, respectively.

The rated power factor of $\cos \varphi_n = 0.8$, specified on the generator nameplate, was used to determine the rated active power of each generator. For the rated apparent power of $\mathbf{S_n = 1320\ kVA}$ given in Table 1, this corresponds to a rated active power of $\mathbf{P_n = 1056\ kW}$. This value was used as the basis for expressing the load of each generator as a percentage.

In the standard load-step tests, the total active and inductive reactive load was increased from 800 kW and 500 kVAr to 1600 kW and 1000 kVAr, respectively, maintaining the same nominal load power factor. These values refer to the total load supplied by both generators. The switching times are indicated in the corresponding plots.

In the first group of experiments, step changes in active and reactive load were applied while both AVRs retained matched settings. The response of the MSB voltage, frequency, active powers, reactive powers, and excitation currents was examined.

In a separate test, the total inductive reactive load was increased from 500 kVAr to 1100 kVAr, while the total active load increased from 800 kW to 900 kW. This predominantly reactive-load increase was used to assess AVR response and reactive power sharing, without reproducing the detailed dynamics of an induction motor.

In the second group of experiments, the effect of differences in the dynamic parameters of the AVRs was analysed. In the first case, the proportional gain was set to its minimum for AVR 1 and its maximum for AVR 2, with all other parameters kept identical and voltage droop properly tuned. In the second case, different integral times were used for the two regulators. These tests aimed to assess the impact of asymmetric dynamics of the two voltage-control loops on the transient reactive power sharing, excitation currents, and damping of oscillations after a load step.

In the next group of tests, the effect of a voltage-setpoint mismatch was analysed. With identical PI settings and voltage droop settings in both AVRs, a small difference in the internal voltage setpoint was introduced between the regulators. In the tested case, this difference was approximately 1 V and was introduced directly by changing the voltage setpoint parameter in the configuration of one of the AVRs. The aim was to evaluate the influence of a small asymmetry in the AVR settings on reactive power sharing, excitation currents, and generator current loading.

The last group of experiments concerned the role of voltage droop in parallel operation. First, the system was tested with different voltage droop settings in the two AVRs, while keeping the tuned PI parameters. Then, a test was performed in which both regulators initially operated with properly tuned parameters, and at time t = 84 s the voltage droop

setting of both AVRs was set to zero. At time t = 105 s, a manual attempt was made to equalise the reactive powers by adjusting the internal voltage setpoints of the AVRs. The objective was to assess the possibility of recovering correct reactive power sharing after disabling the droop function and to observe the associated changes in generator currents. This case is particularly important because it allows observation of the mutual interaction of the regulators via the common MSB under conditions where the function limiting the competitive action of the two voltage loops is absent.

During all tests, the MSB voltage, frequency, active and reactive powers of both generators, excitation currents, and, in selected cases, generator currents were recorded. The assessment was based on a comparison of the transient responses and steady-state values of the measured quantities. Particular attention was paid to the uniformity of reactive power sharing, the occurrence of oscillatory reactive power exchange, the increase in generator currents, and the ability to reach a stable state after a disturbance.

3. Results

3.1. Validation of the Current-Reproduction Interface and Reference Operation

The first stage of the tests involved functional validation of the stator current reproduction interfaces. The aim was to verify that the currents calculated by the real-time models were reproduced as physical current signals supplied to the AVR inputs. The comparison accounted for the scaling described in Section 2.4: the generator currents calculated in the model were converted to the physical current scale by dividing their values by 3810. Amplitude scaling and correction of the reference signal time shift were treated separately. The assessment of current waveform reproduction was supplemented by checking agreement between the power factor calculated in the model and the value indicated by the physical AVR.

Figure 4 shows the stator currents I_{G1} and I_{G2} calculated in the real-time model (upper panel) and the measured inverter output currents I_{INV1} and I_{INV2} (lower panel). The labels I_{G1} and I_{G2} refer to the model currents before scaling and correction of the time shift, rather than to the reference signals of the hysteresis controllers. The current I_{INV} shown for a single channel in Figure 3 corresponds to I_{INV1} or I_{INV2} in Figure 4, depending on the channel. The decrease in the amplitude of the model currents at approximately $t = 330.7$ s is accompanied by a decrease in the amplitude of the inverter currents. Ripple is visible in the lower waveforms. The comparison illustrates the qualitative response of both current reproduction channels to changes in the model currents. No quantitative waveform reproduction error metrics were calculated from this figure.

During commissioning of the test platform, oscillatory reactive power exchange between the generators was observed, including changes in the sign of their reactive powers. At the same time, a discrepancy was identified between the power factor calculated in the real-time model and the value displayed on the LCD panel of the physical AVR. The current reference signal delay was tuned experimentally; a delay of 5.7 ms yielded agreement between the indications and stable operation. Power factor agreement was subsequently checked by monitoring the values in the model and on the AVR display under all tested load conditions. Changes in the model power factor were accompanied by corresponding changes in the AVR indication, without the need to retune the delay. These observations, together with the stable system responses during the reference load changes (Figure 5) and the predominantly reactive-load increase (Section 3.2), supported the functional suitability of the fixed 5.7 ms correction within the tested operating range. No retuning of the delay was required between these tests. Because the LCD readings were not recorded, neither quantitative power factor errors nor their time histories during transients were determined.

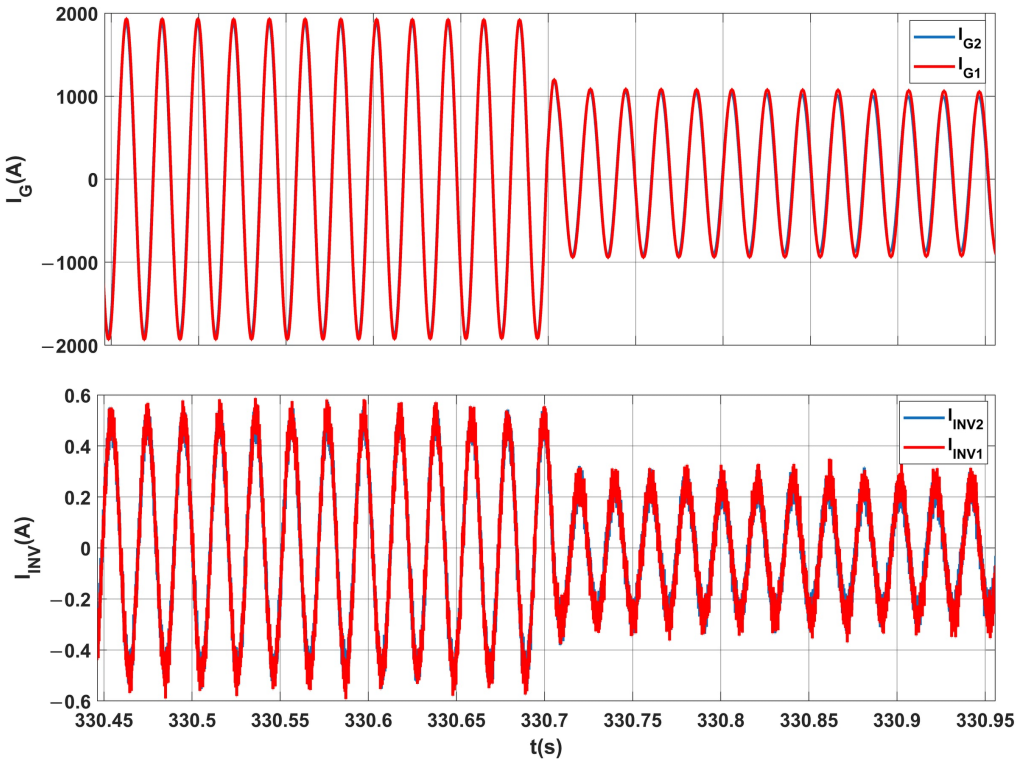


Figure 4. Stator currents I_{G1} and I_{G2} calculated by the generator models (**upper panel**) and measured inverter output currents I_{INV1} and I_{INV2} (**lower panel**) during a load change.

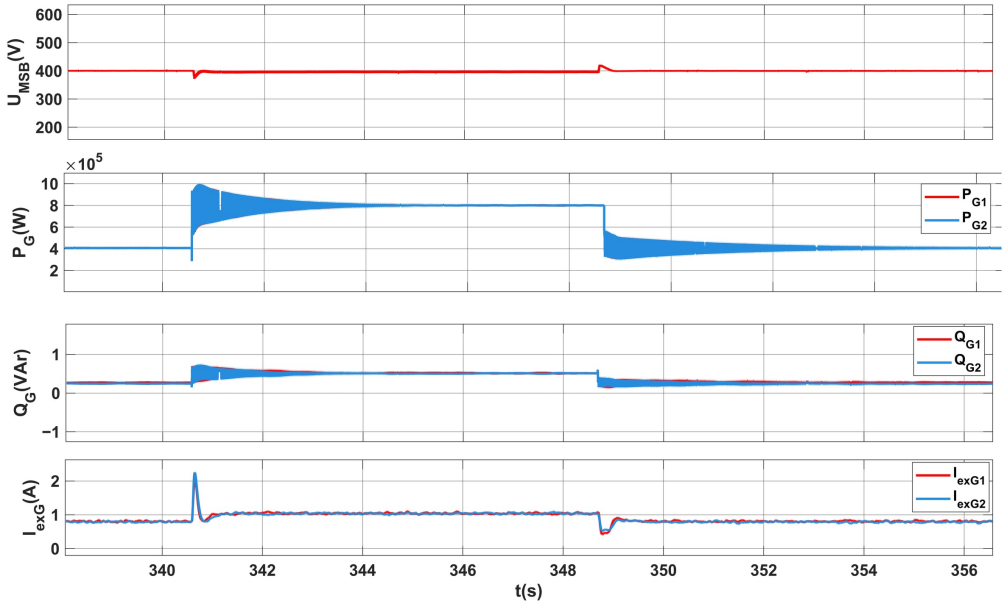


Figure 5. Dynamic response of the parallel shipboard generator system to step load changes with matched AVR parameters and matched voltage droop settings. U_{MSB} denotes the MSB voltage; P_{G1} and P_{G2} are the active powers; Q_{G1} and Q_{G2} are the reactive powers; and I_{exG1} and I_{exG2} are the excitation currents of generators G1 and G2, respectively.

After validating the interfaces, a reference test of two generators operating in parallel with matched AVR settings was performed. In this case, the PI parameters, internal voltage setpoints, and voltage droop of both regulators were identical. The system was subjected to step load changes, and the MSB voltage, active and reactive powers of the generators, and the excitation currents were recorded.

In the reference case, the common MSB voltage remained close to its setpoint during both load changes. The load step caused transient variations in active power, reactive power, and excitation currents, but the response of both regulators was coordinated. After the transient period, the active powers of the generators reached comparable values, and the reactive power sharing remained stable. The excitation currents increased with increasing load and decreased with load reduction, without sustained oscillations. This case serves as a baseline for further assessment of the effects of intentional AVR-setting mismatches.

3.2. Frequency Response and Large Inductive Load

To confirm the operation of the speed governors and their droop characteristics, the change in the common MSB frequency during step load changes was recorded. The waveforms are shown in Figure 6.

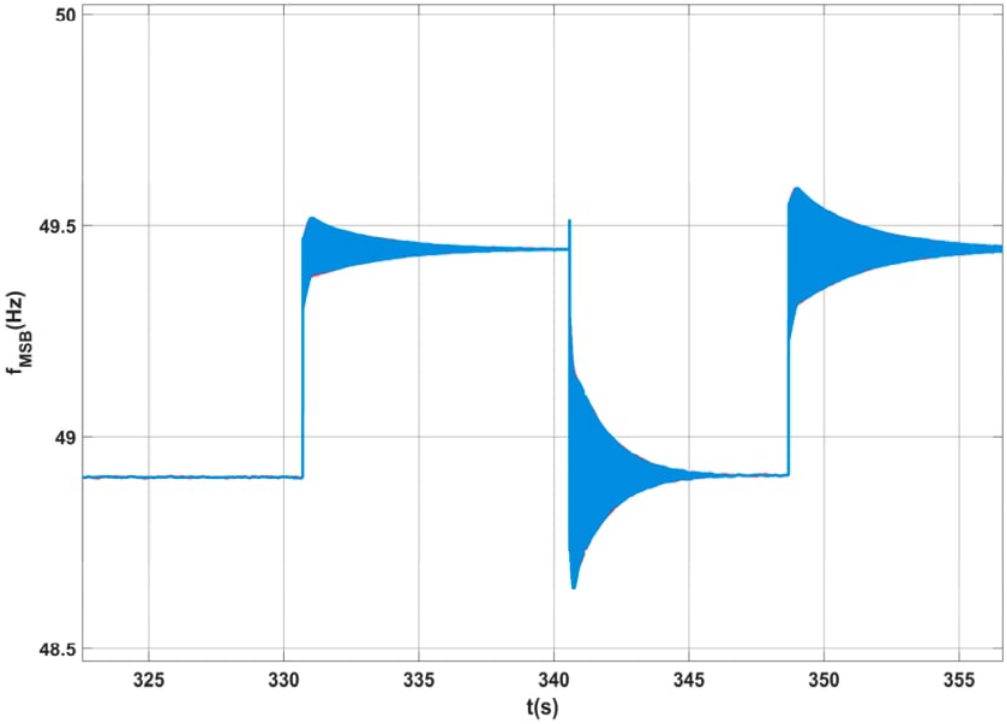


Figure 6. MSB frequency response during load changes, illustrating the action of the speed droop characteristics in the prime-mover models.

Load changes caused short-term frequency deviations, after which the system reached a new steady state. This response confirms the operation of the prime-mover models and speed governors in the parallel arrangement. This result is auxiliary to the AVR tests, as it allows the active power sharing, mainly associated with speed regulation, to be distinguished from the reactive power sharing, which depends on the excitation systems and AVRs.

Next, the predominantly reactive-load increase described in Section 2.5 was applied. The system response is shown in Figure 7.

After connecting the inductive load, the reactive power demand increased, causing an increase in the excitation currents of both generators. Despite the abrupt nature of the disturbance, the MSB voltage was maintained within the regulation range, and both generators participated in supplying reactive power. No sustained asymmetry in reactive power sharing or persistent oscillations was observed. This result indicates that, with

matched AVR settings and properly tuned voltage droop, the HIL platform reproduces a stable response of the parallel system even under a strong inductive disturbance.

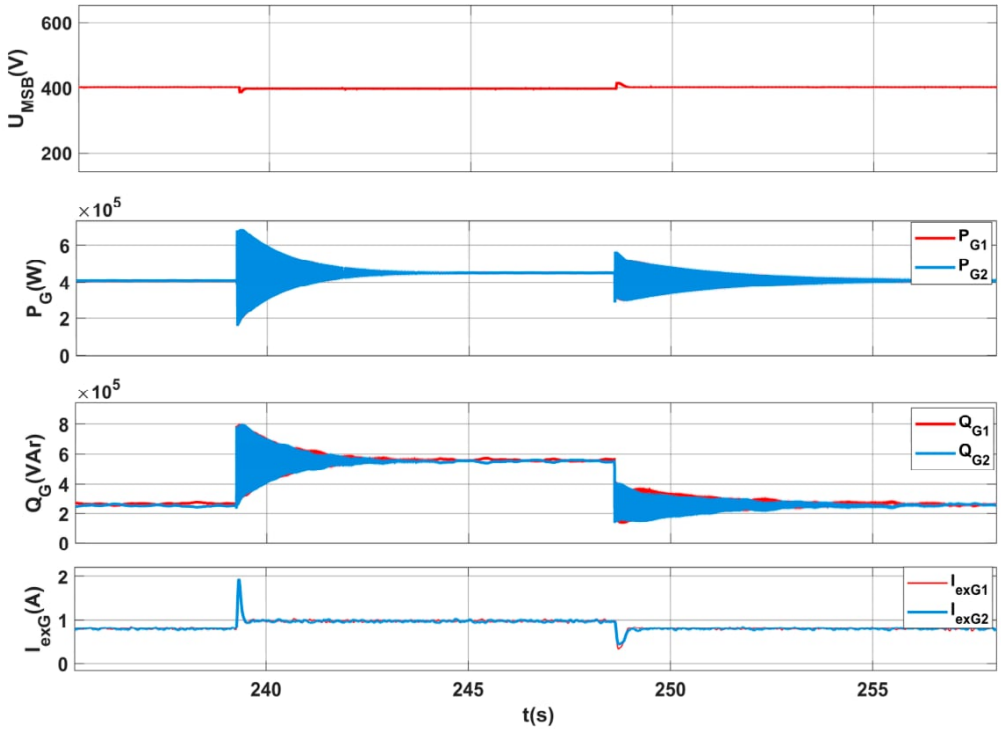


Figure 7. Response to an increase in total inductive reactive load from 500 kVAr to 1100 kVAr and total active load from 800 kW to 900 kW. U_{MSB} denotes the MSB voltage; P_{G1} and P_{G2} are active powers; Q_{G1} and Q_{G2} are reactive powers; and I_{exG1} and I_{exG2} are excitation currents.

3.3. Effect of Mismatched AVR Dynamic Parameters

In the next group of tests, the effect of asymmetry in the dynamic parameters of the AVRs on the system response after a step load change was assessed. In the first test, AVR 1 was set to the minimum proportional gain and AVR 2 to the maximum proportional gain. The other relevant settings, including voltage droop, were kept at the reference level.

Figure 8 shows that different proportional-gain values change the dynamics of the regulators' response to a disturbance. The regulator with higher gain responds faster and more strongly to the instantaneous voltage change, leading to an asymmetric change in the excitation currents of both generators. Consequently, transient oscillations and uneven reactive power exchange occur. With proper voltage droop maintained, these oscillations are, however, limited, and the system recovers a stable reactive power sharing after the transient state decays.

In the second test, different integral times were used for the AVRs while keeping all other operating conditions identical. The response of the system to these settings is shown in Figure 9.

Different integral times caused different speeds of voltage-error elimination by the two regulators. The AVR with the shorter integral time changed the excitation current more quickly and took on a larger share of the transient reactive power change, while the response of the other regulator was delayed. This phenomenon led to temporarily uneven reactive power sharing and higher loading of one of the generators during the transient. After the disturbance, the system nevertheless reached a bounded steady state, indicating that mismatched integral times alone, with voltage droop maintained, did not cause a permanent loss of stability.

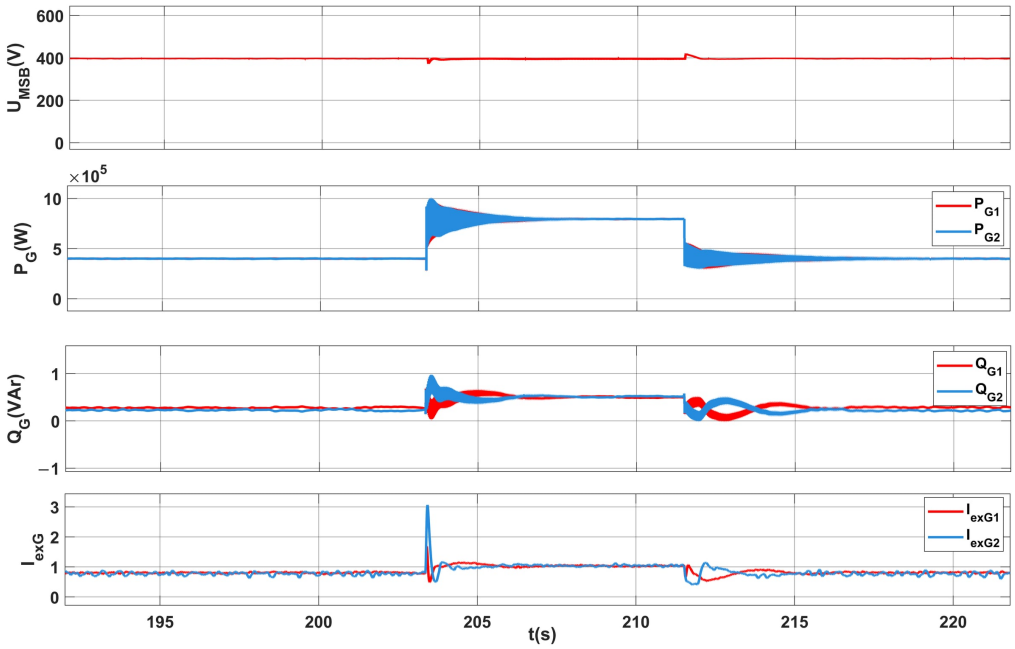


Figure 8. Response to step load changes with mismatched proportional-gain settings: minimum proportional gain in AVR 1 and maximum proportional gain in AVR 2, with matched voltage droop settings.

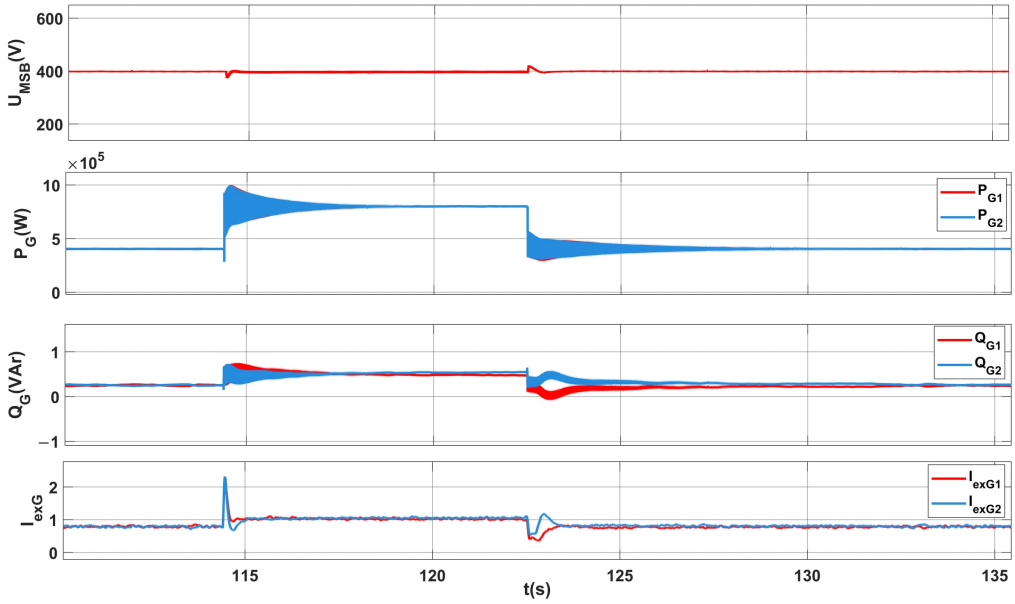


Figure 9. Response to step load changes with mismatched integral-time settings: minimum integral time in AVR 1 and maximum integral time in AVR 2, with matched voltage droop settings.

To assess the combined effect of differences in regulator dynamics and weakening of the reactive power sharing mechanism, a test was performed with asymmetric settings and minimum voltage droop. The corresponding waveforms are presented in Figure 10.

In this case, reducing the voltage droop decreased the system's ability to establish a unique and stable reactive power sharing after a load change. Compared with the case shown in Figure 8, the oscillatory reactive power exchange was more pronounced and less damped. This result indicates that properly tuned voltage droop limits the competitive interaction of the two AVRs acting on the common MSB.

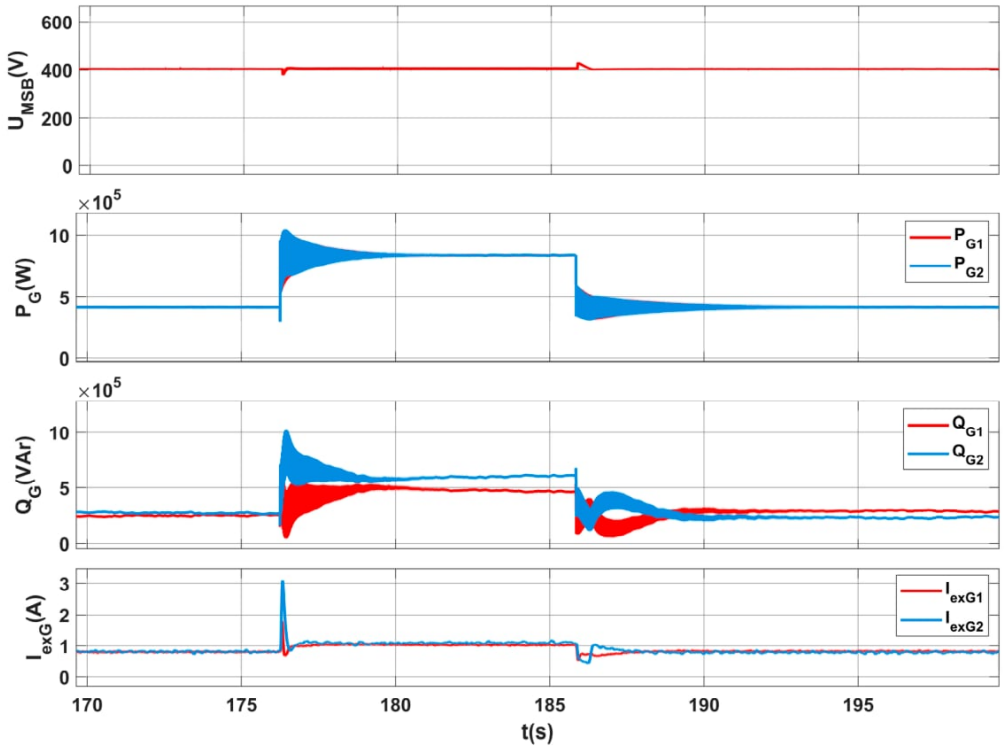


Figure 10. Combined effect of mismatched proportional-gain settings and minimum voltage droop setting on the response of parallel shipboard generators.

3.4. Effect of Voltage Setpoint and Voltage Droop Differences

The next test assessed the effect of a small difference between the internal voltage setpoints of the AVRs on reactive power sharing between the generators operating in parallel. With identical PI controller and voltage droop settings, the internal voltage setpoint of one AVR was adjusted to produce a setpoint difference of approximately 1 V. The aim of the test was to demonstrate the sensitivity of reactive power sharing to a small difference in voltage setpoints. The stated difference refers to the setpoints within the AVRs, not to a difference between the terminal voltages of the generators connected to the common MSB bus. The MSB voltage, active and reactive powers, and excitation currents recorded during this test are shown in Figure 11. The waveforms illustrate the development of a persistent asymmetry in reactive power sharing following the introduction of the voltage-reference mismatch.

Despite the small change in the setpoint, a significant asymmetry in reactive power sharing was observed. The regulator with the higher setpoint increased excitation, tending to raise the common bus voltage, while the other regulator reduced excitation. As a result, one generator took on a larger share of the reactive power, and the other was driven towards underexcited operation. The MSB voltage could simultaneously remain close to its setpoint, so the MSB voltage measurement alone is not a sufficient indicator of correct generator cooperation. The result confirms the high sensitivity of the parallel system to small differences in the internal AVR voltage setpoints.

The next test concerned different voltage droop settings in the two regulators, with identical PI parameters.

Figure 12 shows that different voltage droop characteristics can lead to uneven reactive power sharing even in steady state. The generator with the smaller droop, i.e., with a stiffer voltage characteristic, takes on a larger share of the reactive power. The system may remain stable in terms of MSB voltage, but long-term asymmetry in reactive loading causes uneven current loading of the generators. This result indicates that monitoring only the

MSB voltage is not sufficient; during commissioning and servicing, the consistency of the droop characteristics of both AVRs should also be verified.

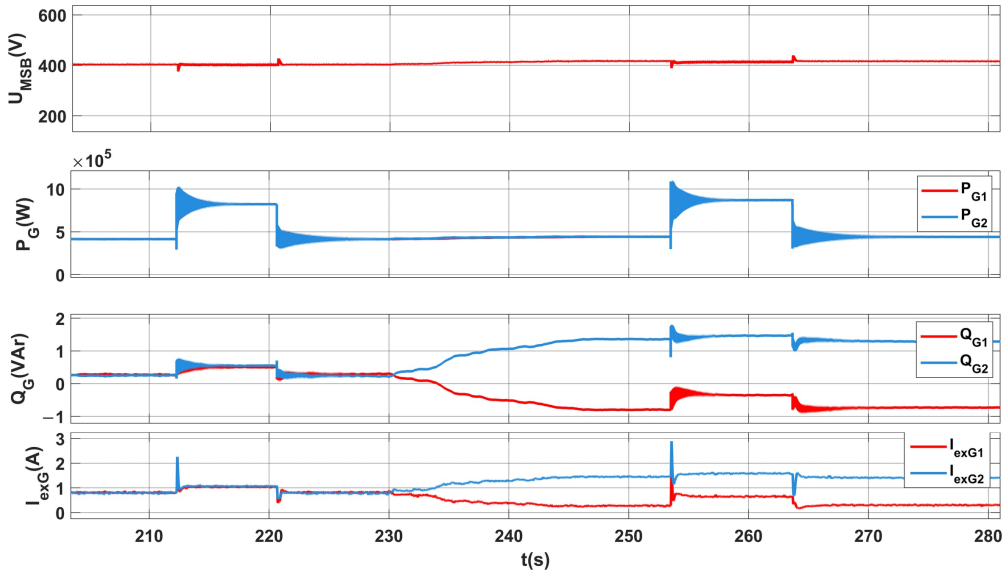


Figure 11. Effect of an approximately 1 V mismatch between the internal voltage-reference settings of AVR 1 and AVR 2, with matched PI and voltage droop settings.

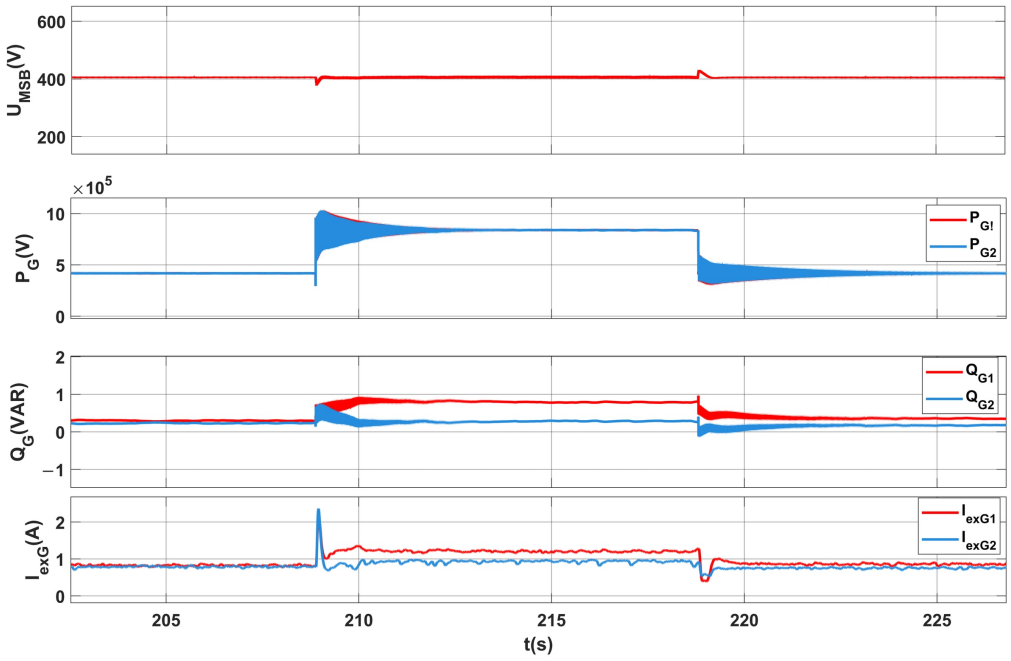


Figure 12. Unequal steady-state reactive power sharing caused by mismatched voltage droop settings, with matched PI parameters.

3.5. Operation with Zero Voltage Droop

The final test concerned parallel operation of the generators after the voltage droop settings of both AVRs were set to zero. Until t = 84 s, the system operated with the reference settings. At t = 84 s, the operator manually set the voltage droop settings of both AVRs to zero. The timing of this change was not predetermined. Subsequently, at t = 105 s, a manual attempt to equalise reactive power sharing was initiated by adjusting the internal voltage setpoints of the AVRs.

Voltage setpoint adjustment was chosen because it is readily available during operation and maintenance as a means of manually correcting reactive power sharing between parallel generators.

The system load remained constant while the voltage droop settings were set to zero and during the subsequent manual voltage setpoint adjustments. After the voltage droop settings had been set to zero, the voltage setpoints were the only AVR settings adjusted. The waveforms recorded during this test are shown in Figure 13.

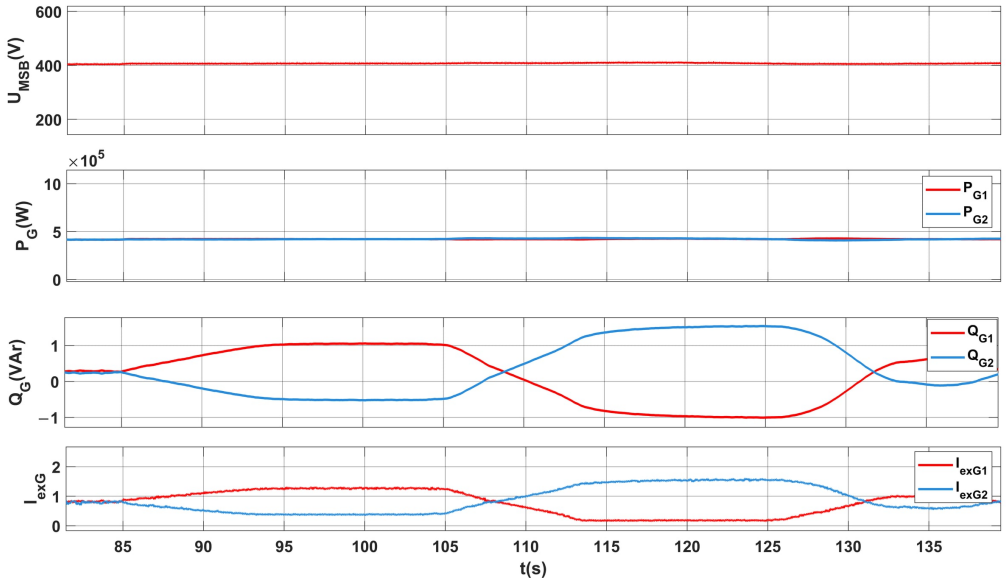


Figure 13. Response of the parallel generator system after voltage droop was set to zero in both AVRs at $t = 84$ s. A manual attempt to restore reactive power sharing by adjustment of the internal AVR voltage-reference settings was performed at $t = 105$ s.

After the voltage droop settings were set to zero, oscillatory reactive power exchange between the generators was observed. Manual adjustment of the voltage setpoints, initiated at $t = 105$ s, did not achieve a lasting balance in reactive power sharing or eliminate the oscillations within the recorded time interval. Because the system load remained constant, the observed changes in reactive power sharing were not caused by changes in load demand. In the analysed case, manual adjustment of the voltage setpoints did not replace the action of a properly configured voltage droop function. The generator current waveforms recorded during the same test are shown in Figure 14. They illustrate the increase in generator currents associated with the sustained oscillatory reactive power exchange after the voltage droop settings were set to zero.

The generator currents increased along with the sustained oscillatory exchange of reactive power. This current increase was due to internal circulation of reactive power between the parallel-operated generators, rather than to a change in load demand. For generator G2, the reactive component of the current included both the component associated with the load and the component resulting from reactive power exchange with the other generator. Such a condition can lead to current overload, activation of protection devices, and loss of available power reserve. If one generator is disconnected under conditions of insufficient reserve in the other set, the risk of a supply-interruption event, including blackout, may increase.

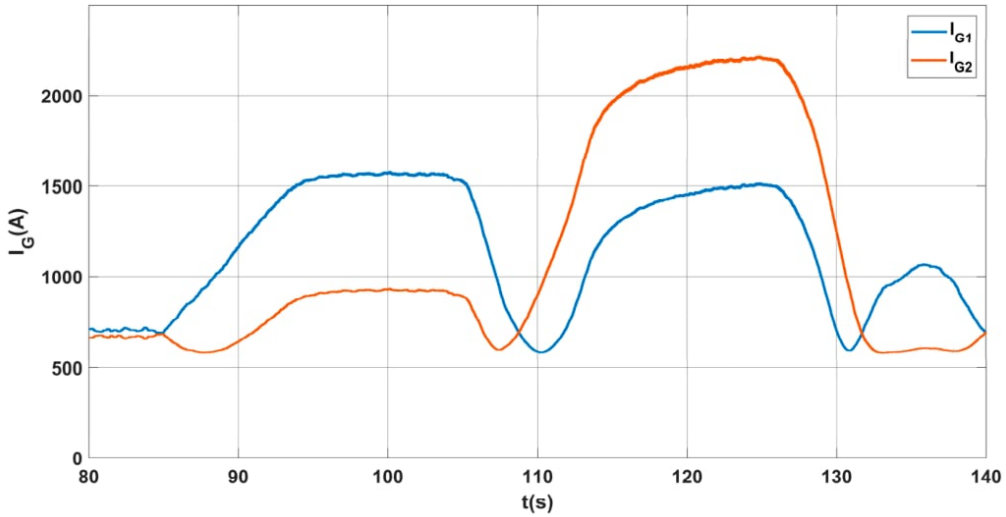


Figure 14. Generator-current response during operation with zero voltage droop. The currents were recorded for the same test presented in Figure 13.

4. Discussion

The experimental results confirmed that the developed HIL platform can be used to analyse the interaction of two physical digital AVRs connected to a real-time model of parallel-operating synchronous generators. Functional validation of the stator current reproduction interface confirmed that the currents calculated by the real-time generator models could be reproduced as physical input signals for the AVRs. Correct phase alignment between voltage and current was a necessary condition for proper interface operation. Adjustment of the current-reference delay provided observed agreement between the power factor calculated by the model and the value indicated on the AVR display under the tested load conditions.

The reference case provided a baseline for assessing the effect of intentional setting mismatches. With matched PI parameters, voltage setpoints, and voltage droop characteristics, the system maintained the common MSB voltage close to its reference value and achieved stable reactive power sharing after load changes. A similar response was obtained during a strong inductive disturbance. This confirms that, in the tested configuration, properly tuned AVR settings enabled coordinated operation of both regulators even during a rapid change in reactive power demand.

The results show a clear distinction between the effects of dynamic parameters and those of settings that define the steady-state characteristic of the regulators. Differences in proportional gain and integral time mainly changed the speed of response and the transient distribution of reactive power. The regulator with higher gain or shorter integral time responded faster. The associated generator then took a larger share of the instantaneous reactive power change. With correct voltage droop, this asymmetry was limited after the transient.

The effect of voltage droop is not limited to determining steady-state reactive power sharing. Voltage droop introduces negative feedback into the voltage control loop that depends on the reactive component of the generator current. If, following a disturbance, one generator temporarily supplies a larger share of the reactive load, the associated droop correction limits its tendency to increase excitation further. For the generator supplying less reactive power, the correction is correspondingly smaller. This mechanism counteracts the growth of the reactive load imbalance and limits the competing action of the two regulators responding to the common bus voltage.

With zero voltage droop, this corrective mechanism is absent. Differences in the dynamic responses of the PI controllers, together with small asymmetries in setpoints

or measurement paths, may then excite oscillatory reactive power exchange between the generators. Nonzero voltage droop changes the coupling between the two control loops and may limit this exchange, but it does not replace appropriate PI controller tuning or guarantee stability for arbitrary controller parameters. The results presented apply to the tested configuration and range of settings.

Differences in internal voltage setpoints and in voltage droop settings had a different character. Even a small mismatch in voltage setpoints caused a persistent change in the share of reactive power supplied by each generator. Different droop characteristics also led to unequal sharing in steady state. In the tested configuration, the generator with the smaller droop took a larger share of reactive power. These results indicate that consistency of static settings is essential for balanced generator loading.

The case with zero voltage droop was particularly significant. After disabling this function, persistent oscillatory reactive power exchange within the recorded interval was observed. Manual adjustment of voltage setpoints did not restore a stable steady state. The accompanying increase in generator currents resulted from internal circulation of reactive power, not from an increase in load demand. In the analysed system, manual setpoint correction did not replace a correctly configured droop mechanism.

The study also shows that monitoring only the MSB voltage is insufficient to assess generator cooperation. The common-bus voltage can remain close to its setpoint while reactive power sharing is uneven, one generator operates in an underexcited region, or circulating currents increase. Commissioning and maintenance procedures should therefore analyse voltage, reactive power, excitation current, generator current, and power factor together.

Based on the literature review, no experimental HIL studies were identified that systematically analysed the effect of mismatch between two physical commercial digital AVRs cooperating with synchronous generators in an isolated shipboard network. In this respect, the present work complements existing studies on reactive power sharing in shipboard microgrids, which focus mainly on power-electronic sources and advanced control algorithms.

The study has a limited scope. It covered two parallel-operating generators and AVRs using quadrature droop compensation. Other regulator types, larger numbers of generating sets, and all protection and power-plant configurations encountered on ships were not analysed. Part of the system was represented by a real-time model, so quantitative results depend on the fidelity of the generator, excitation, load, and network models. These limitations must be considered when transferring the results to specific installations. They do not invalidate the identified qualitative mechanism: AVR setting mismatches can cause unequal reactive power sharing and increased generator current loading.

From a practical viewpoint, the developed HIL platform enables safe and repeatable testing of AVRs without using high-power physical generators and without disturbing an operating shipboard network. It can be used for diagnostics, commissioning, functional testing, and post-repair verification. Detection of incorrect regulator coordination is important because reactive power circulation can reduce the loading margin of generators and increase the likelihood of limiter or protection operation. Such a condition can occur even when the common-bus voltage remains close to its setpoint.

Within the scope represented by the model, HIL test results can be used to assess AVR functionality, compare parameter configurations, and identify settings that lead to undesirable oscillations or unequal reactive power sharing. They can also provide a basis for selecting preliminary settings and scenarios for further testing on the actual system. However, this does not imply that PI controller and voltage droop settings can be transferred directly to any shipboard generator. Such use requires confirmation that the model adequately represents the specific installation, particularly with respect to generator and excitation system parameters, measurement paths, time delays, and network configuration.

Preliminary settings selected on the basis of HIL tests should be verified during controlled trials on the actual vessel, taking the manufacturer's requirements into account. The platform therefore supports the preparation and planning of the tuning process but does not replace final verification on board.

5. Conclusions

This work developed and functionally validated an HIL platform for studying the interaction of two physical digital AVRs connected to a real-time model of parallel-operating synchronous generators in a shipboard network. The platform enabled analysis of the closed-loop interaction between the regulators, common-bus voltage, stator currents, and excitation currents.

Validation of the current interface confirmed that the signals required by the physical AVRs could be reproduced. After adjustment of the current-reference delay, agreement between the model power factor and the AVR display indication was observed throughout the tested load conditions. This condition was necessary for correct representation of the voltage droop function.

In the tested configuration, matched regulator settings ensured stable operation after load changes, including during a strong inductive disturbance. Mismatch of dynamic parameters mainly affected the transient response. Differences in voltage setpoints and voltage droop settings could cause persistent asymmetry in reactive power sharing.

Setting the voltage droop to zero led to oscillatory reactive power exchange and increased generator currents due to internal circulation of reactive power. The results show that correct common-bus voltage is not a sufficient criterion for assessing generator cooperation. Diagnostics and commissioning should also consider reactive power, excitation currents, generator currents, and power factor.

The proposed method enables safe and repeatable testing and is intended to support commissioning and post-repair verification of digital AVRs without using high-power generators. The quantitative results apply to the analysed configuration of two generators and AVRs using quadrature droop compensation. Further work should consider larger numbers of generators, other regulator and protection architectures, and the effect of speed-governor dynamics on generator cooperation.

Author Contributions: Conceptualization, T.Z., D.T., Z.M., M.J. and R.P.; methodology, T.Z. and D.T.; software, T.Z. and D.T.; validation, T.Z., D.T., Z.M., M.J. and R.P.; formal analysis, T.Z. and D.T.; investigation, T.Z. and D.T.; data curation, T.Z. and D.T.; writing—original draft preparation, T.Z. and D.T.; writing—review and editing, T.Z., D.T. and R.P.; visualisation, T.Z. and D.T.; supervision, T.Z., D.T., Z.M., M.J. and R.P. All authors have read and agreed to the published version of the manuscript.

Funding: This research received no external funding.

Data Availability Statement: The original contributions presented in this study are included in the article. Further inquiries can be directed to the corresponding author.

Conflicts of Interest: The authors declare no conflicts of interest.

References

1. Boyd, G.; Taylor, F. *Electrical Power Systems for Marine Engineers*; Reeds Marine Engineering and Technology Series; Bloomsbury Publishing: London, UK, 2020.
2. Patel, M.R. *Shipboard Electrical Power Systems*, 2nd ed.; CRC Press: Boca Raton, FL, USA, 2022.
3. Śmierzchalski, R. *Automation of the Ship's Power System*; Graphics Center Gryf: Gdańsk, Poland, 2004.
4. Al-Falahi, M.D.A.; Tarasiuk, T.; Jayasinghe, S.G.; Jin, Z.; Enshaei, H.; Guerrero, J.M. AC Ship Microgrids: Control and Power Management Optimization. *Energies* **2018**, *11*, 1458. [CrossRef]

5. Prousalidis, J.M.; Xanthopoulos, E.; Voutzoulidis, K. Reactive Power Sharing in Ship Energy Systems with Shaft Generators. *J. Mar. Eng. Technol.* **2009**, *2009*, 21–38. [CrossRef]
6. Ochoa, D.; Martinez, S. Proposals for Enhancing Frequency Control in Weak and Isolated Power Systems: Application to the Wind-Diesel Power System of San Cristobal Island-Ecuador. *Energies* **2018**, *11*, 910. [CrossRef]
7. Tarnapowicz, D. Load Analysis of Ship Generating Sets During the Maneuvers of the Vessel. In *Current Methods of Construction Design*; Medvecký, Š., Hrček, S., Kohár, R., Brumerčík, F., Konstantová, V., Eds.; Springer: Cham, Switzerland, 2020; pp. 399–407. [CrossRef]
8. Parise, G. Service Continuity in Complex Power Systems: Safety, Operation and Reliability of Multi-Source Electrical Networks. Doctoral Dissertation, Sapienza University of Rome, Rome, Italy, 2014.
9. Tarnapowicz, D. Synchronization of National Grid Network with the Electricity Ships Network in the "Shore to Ship" System. *Manag. Syst. Prod. Eng.* **2013**, *12*, 9–13.
10. Cimino, M.; Pagilla, P.R. Reactive Power Control for Multiple Synchronous Generators Connected in Parallel. *IEEE Trans. Power Syst.* **2016**, *31*, 4371–4378. [CrossRef]
11. Kundur, P.; Balu, N.J.; Lauby, M.G. *Power System Stability and Control*; McGraw-Hill: New York, NY, USA, 1994.
12. Anderson, P.M.; Fouad, A.A. *Power System Control and Stability*, 2nd ed.; IEEE Press/Wiley-Interscience: Piscataway, NJ, USA, 2003.
13. Machowski, J.; Białek, J.W.; Bumby, J.R. *Power System Dynamics: Stability and Control*, 3rd ed.; Wiley: Chichester, UK, 2020.
14. Nicewicz, G.; Sosiński, M.; Tarnapowicz, D. Identification of Power Factor in Marine Electrical Grid. In Proceedings of the 14th International Multidisciplinary Scientific GeoConference SGEM 2014, Albena, Bulgaria, 17–26 June 2014; pp. 393–400. [CrossRef]
15. Pota, H.R. Design of the Automatic Voltage Regulator. In *The Essentials of Power System Dynamics and Control*; Springer: Singapore, 2018; pp. 1–31.
16. Yegireddy, N.K.; Panda, S.; Tentu, P.; Durgamalleswarao, K. Comparative Analysis of PID Controller for an Automatic Voltage Regulator System. In *Proceedings of the International Conference on Electrical, Electronics, Signals, Communication and Optimization (EESCO), Visakhapatnam, India, 24–25 January 2015*; IEEE: Piscataway, NJ, USA, 2015. [CrossRef]
17. Ghamri, L.Y.; Awadh, H.; Al Shamsi, N.; AlKhateri, S.; Khurram, A.; Rehman, H. Robust AVR Design for the Synchronous Generator. *J. Eng.* **2019**, *2019*, 4111–4115. [CrossRef]
18. Sokólski, P.; Rutkowski, T.A.; Dużinkiewicz, K. The Excitation Controller with Gain Scheduling Mechanism for Synchronous Generator Control. In Proceedings of the 20th International Conference on Methods and Models in Automation and Robotics (MMAR), Międzyzdroje, Poland, 24–27 August 2015; pp. 23–28. [CrossRef]
19. Guerrero, J.M.; Vasquez, J.C.; Matas, J.; de Vicuña, L.G.; Castilla, M. Hierarchical Control of Droop-Controlled AC and DC Microgrids-A General Approach toward Standardization. *IEEE Trans. Ind. Electron.* **2011**, *58*, 158–172. [CrossRef]
20. Guerrero, J.M.; Chandorkar, M.; Lee, T.-L.; Loh, P.C. Advanced Control Architectures for Intelligent Microgrids-Part I: Decentralized and Hierarchical Control. *IEEE Trans. Ind. Electron.* **2013**, *60*, 1254–1262. [CrossRef]
21. Simpson-Porco, J.W.; Dörfler, F.; Bullo, F. Synchronization and Power Sharing for Droop-Controlled Inverters in Islanded Microgrids. *Automatica* **2013**, *49*, 2603–2611. [CrossRef]
22. Micallef, A.; Apap, M.; Spiteri-Staines, C.; Guerrero, J.M.; Vasquez, J.C. Reactive Power Sharing and Voltage Harmonic Distortion Compensation of Droop Controlled Single Phase Islanded Microgrids. *IEEE Trans. Smart Grid* **2014**, *5*, 1149–1158. [CrossRef]
23. Zhong, Q.-C. Robust Droop Controller for Accurate Proportional Load Sharing Among Inverters Operated in Parallel. *IEEE Trans. Ind. Electron.* **2013**, *60*, 1281–1290. [CrossRef]
24. Tarnapowicz, D.; German-Galkin, S.; Staude, M. Investigation Concerning the Excitation Loss of Synchronous Generators in a Stand-Alone Ship Power Plant. *Energies* **2021**, *14*, 2828. [CrossRef]
25. Baracho, F.R.A.C.; Coelho, A.L.M.; Damião, L.J.S.; Zvietcovich, W.G. Real-Time Digital Simulation for Coordination Analysis of V/Hz AVR Limiter With Overexcitation, Overvoltage, and Underfrequency Protections of Synchronous Generators. *IEEE Trans. Ind. Appl.* **2022**, *58*, 3361–3369. [CrossRef]
26. Tarnapowicz, D.; Zaleski, T.; Matuszak, Z.; Jaskiewicz, M.; Sawicki, S. Testing the Automatic Voltage Regulators of Ship Synchronous Generators Using Hardware-in-the-Loop Technology. *Energies* **2024**, *17*, 5963. [CrossRef]
27. Meng, L.; Yang, S.; Wang, L.; Liu, Y.; Peng, F. Hardware-in-Loop Test for Automatic Voltage Regulator Based on Identification Model. In Proceedings of the 15th International Power Electronics and Motion Control Conference (EPE/PEMC), Novi Sad, Serbia, 4–6 September 2012; pp. DS1e.2-1–DS1e.2-6. [CrossRef]
28. Comelli, R.; Calvizi, M.E.; Romero, P.A.M. Real-Time Synchronous Machine Simulator for Testing of Automatic Voltage Regulators. In *Proceedings of the 2018 Argentine Conference on Automatic Control (AADECA), Buenos Aires, Argentina, 7–9 November 2018*; IEEE: Piscataway, NJ, USA, 2018; pp. 1–6. [CrossRef]
29. Almas, M.S.; Vanfretti, L. RT-HIL Testing of an Excitation Control System for Oscillation Damping Using External Stabilizing Signals. In *Proceedings of the 2015 IEEE Power & Energy Society General Meeting, Denver, CO, USA, 26–30 July 2015*; IEEE: Piscataway, NJ, USA, 2015; pp. 1–5. [CrossRef]

30. Nguyen, H.T.; Yang, G.; Nielsen, A.H.; Jensen, P.H. Hardware-in-the-Loop Test for Automatic Voltage Regulator of Synchronous Condenser. *Int. J. Electr. Electron. Commun. Sci.* **2018**, *12*, 181–186.
31. Coelho, A.L.M.; Silveira, P.M.; Baracho, F.R.A.C.A. Test-Bed for Protection Studies of Synchronous Generators and Its Interaction with the Underexcitation and Overexcitation Limiters. In *Proceedings of the 2018 IEEE Industry Applications Society Annual Meeting, Portland, OR, USA, 23–27 September 2018*; IEEE: Piscataway, NJ, USA, 2018; pp. 1–12. [CrossRef]
32. Crăciun, O.; Florescu, A.; Bacha, S.; Munteanu, J.; Bratcu, A.J. Hardware-in-the-Loop Testing of PV Control Systems Using RT-LAB Simulator. In Proceedings of the 14th International Power Electronics and Motion Control Conference, Ohrid, North Macedonia, 6–8 September 2010; pp. S2-1–S2-6.
33. Ren, W.; Sloderbeck, M.; Steurer, M.; Dinavahi, V.; Noda, T.; Filizadeh, S.; Chevrefils, A.R.; Matar, M.; Iravani, R.; Dufour, C.; et al. Interfacing Issues in Real-Time Digital Simulators. *IEEE Trans. Power Deliv.* **2011**, *26*, 1221–1230. [CrossRef]
34. Palensky, P.; van der Meer, A.A.; Lopez, C.; Joseph, A.; Pan, K. Cosimulation of Intelligent Power Systems: Fundamentals, Software Architecture, Numerics, and Coupling. *IEEE Ind. Electron. Mag.* **2017**, *11*, 34–50. [CrossRef]
35. Strasser, T.; Andrén, F.; Kathan, J.; Cecati, C.; Buccella, C.; Siano, P.; Leitão, P.; Zhabelova, G.; Vyatkin, V.; Zhivich, M.; et al. A Review of Architectures and Concepts for Intelligence in Future Electric Energy Systems. *IEEE Trans. Ind. Electron.* **2015**, *62*, 2424–2438. [CrossRef]
36. Pogaku, N.; Prodanović, M.; Green, T.C. Modeling, Analysis and Testing of Autonomous Operation of an Inverter-Based Microgrid. *IEEE Trans. Power Electron.* **2007**, *22*, 613–625. [CrossRef]
37. Shi, K.; Song, W.; Ge, H.; Xu, P.; Yang, Y.; Blaabjerg, F. Transient Analysis of Microgrids with Parallel Synchronous Generators and Virtual Synchronous Generators. *IEEE Trans. Energy Convers.* **2020**, *35*, 95–105. [CrossRef]
38. Peng, Y.; Shuai, Z.; Huang, W.; Shen, X. Design-Oriented Analysis and Enhancement of Transient Power Sharing Between Inverter-Interfaced Generators and Synchronous Generators. *CSEE J. Power Energy Syst.* **2025**, *11*, 2349–2359. [CrossRef]
39. Kutsyk, A.; Semeniuk, M.; Korkosz, M.; Podskarbi, G. Diagnosis of the Static Excitation Systems of Synchronous Generators with the Use of Hardware-In-the-Loop Technologies. *Energies* **2021**, *14*, 6937. [CrossRef]
40. Racewicz, S.; Kutt, F.; Sienkiewicz, Ł. Power Hardware-In-the-Loop Approach for Autonomous Power Generation System Analysis. *Energies* **2022**, *15*, 1720. [CrossRef]
41. Kutt, F.; Sienkiewicz, Ł.; Racewicz, S.; Michna, M.; Ryndzionek, R. Development of an emulation platform for synchronous machine power generation system using a nonlinear functional level model. *Arch. Electr. Eng.* **2024**, *73*, 281–297. [CrossRef]
42. von Jouanne, A.; Agamloh, E.; Yokochi, A. Power Hardware-in-the-Loop (PHIL): A Review to Advance Smart Inverter-Based Grid-Edge Solutions. *Energies* **2023**, *16*, 916. [CrossRef]
43. Mihalič, F.; Truntič, M.; Hren, A. Hardware-in-the-Loop Simulations: A Historical Overview of Engineering Challenges. *Electronics* **2022**, *11*, 2462. [CrossRef]
44. Li, W.; Zhao, H.; Zhu, J.; Yang, T. A Novel Reactive Power Sharing Control Strategy for Shipboard Microgrids Based on Deep Reinforcement Learning. *J. Mar. Sci. Eng.* **2025**, *13*, 718. [CrossRef]
45. Li, Y.; Vilathgamuwa, D.M.; Loh, P.C. Design, Analysis, and Real-Time Testing of a Controller for Multibus Microgrid System. *IEEE Trans. Power Electron.* **2004**, *19*, 1195–1204. [CrossRef]
46. Li, Y.; Deng, F.; Qi, R.; Lin, H. Adaptive Virtual Impedance Regulation Strategy for Reactive and Harmonic Power Sharing among Paralleled Virtual Synchronous Generators. *Int. J. Electr. Power Energy Syst.* **2022**, *140*, 108059. [CrossRef]

Disclaimer/Publisher's Note: The statements, opinions and data contained in all publications are solely those of the individual author(s) and contributor(s) and not of MDPI and/or the editor(s). MDPI and/or the editor(s) disclaim responsibility for any injury to people or property resulting from any ideas, methods, instructions or products referred to in the content.